Available online at www.eccomasproceedia.org
Eccomas Proceedia COMPDYN (2021) 779-794

ECCOMAS
Proceedia

COMPDYN 2021
8th ECCOMAS Thematic Conference on
Computational Methods in Structural Dynamics and Earthquake Engineering
M. Papadrakakis, M. Fragiadakis (eds.)
Streamed from Athens, Greece, 28 - 30 June 2021

NUMERICAL MESO-MODEL FOR REINFORCED CONCRETE FRAMES WITH RETROFITTED MASONRY INFILL

Gianni Blasi[1], Daniele Perrone[1,2], Maria Antonietta Aiello[1].

[1]University of Salento, Italy, {gianni.blasi, daniele.perrone, antonietta.aiello}@unisalento.it

[2]University School for Advanced Studies, Italy, daniele.perrone@iusspavia.it

Abstract

Several research outcomes have ascertained the need of considering the infill walls in the dynamic response evaluation of reinforced concrete framed buildings. In the case of buildings designed prior the introduction of modern seismic codes, the presence of strong infill might highly influence the failure mode in case of earthquake. Furthermore, considering the increasingly adoption of retrofit techniques aimed at enhancing the in-plane and out-of-plane capacity of the infill walls, its influence on the seismic performance of the structure should be investigated at global and local level. In this study, a numerical model to simulate the response to lateral loads of reinforced concrete frames with retrofitted masonry infill walls is developed. Particularly, since the use of composites is widespread due to the well-known benefits of these materials, the work is focused on the in-plane infill retrofit by fibre-reinforced polymer (FRP). The proposed model for the retrofitted infill is validated by numerical simulation of diagonal compression tests on masonry panels previously conducted at university of Salento. Aiming to analyse the influence of the retrofit on the seismic performance of the frame, the retrofitted infill and unreinforced infill performances are compared. Depending on the infill type considered, the failure modes of the frame members, the energy dissipated under lateral loading and the displacement capacity are analysed.

Keywords: Meso-modelling, Infilled frames, retrofitted infill, seismic vulnerability, RC frames.

ISSN:2623-3347
Peer-review under responsibility of the organizing committee of COMPDYN 2021.
doi:10.7712/120121.8525.18704

1 INTRODUCTION

The in-plane or out-of-plane collapse of infill walls caused by earthquakes can represent a major threat for life safety, particularly during seismic emergency. Moreover, the seismic damage on infills might cause in-direct losses which affect the serviceability of the building, such as failure of piping lines or electrical wiring embedded in the walls. The severe damage on masonry infill walls, documented in several post-seismic on-site recognitions [1–3], led to recent investigations through laboratory tests [4–6] and numerical studies [7,8], with the scope of characterizing their seismic response. Aiming to avoid infill's damage due to earthquake, state-of-art retrofit solutions are increasingly employed on existing buildings. Textile-Reinforced Mortar (TRM), Composite-Reinforced-Mortar (CRM) or Steel-Reinforced-Grout (SRG) jacketing significantly increase the lateral load capacity of masonry panels [9–11], even though such techniques are not always applicable due to the mass and thickness increase. On the other hand, the use of fibre-reinforced polymers (FRP) retrofit prevents out-of-plane failure and increases the in-plane tensile strength of the wall without majorly modifying its thickness [12,13].

The increasingly number of studies on strengthened masonry walls allowed to comprehensively define their in-plane and out-of-plane response, as well as the failure modes in case of lateral loading. Several analytical models were calibrated based on experimental findings, contributing to the development of guidelines for retrofit techniques [14,15], which provide instruction for their design, installation and maintenance. Most of the studies on strengthened panels are addressed to load-bearing walls in masonry structures, which are widespread in Mediterranean regions and represent a building category with high seismic vulnerability. On the other hand, the research outcome also applies to non-structural masonry panels in RC framed structures. To this regard, despite the strengthening techniques adopted for infill walls are generally identical to those used in masonry structures, additional considerations are required in the former case to account for the frame-infill interaction.

The influence of the infills on the dynamic performance of RC framed structures is well-known in earthquake engineering. Several studies provided simplified formulations to simulate the lateral behaviour of infilled frames and to predict the seismic demand depending on the properties of the masonry walls [16,17]. Additionally, the analysis of the effect of the infills on the seismic behaviour of RC frames is addressed in recent building codes [18–20]. In the case of buildings built before the introduction of modern seismic design codes, the presence of strong infill walls not only provides a significant contribution to the lateral stiffness, but can also influence the failure mode of the frame members [21–23]. The additional shear demand in columns with poor shear reinforcement caused by the infill-frame interaction can lead to early brittle failure and, consequently, reduce the displacement and ductility capacity of the RC structures [24].

Since the retrofit techniques currently used to prevent non-structural walls collapse significantly increase their lateral strength, an accurate evaluation of the consequences of the retrofit on the structural performance is strictly required when dealing with gravity load designed RC frames. In fact, a shear strengthening of the columns might be also required, in order to avoid brittle failure caused by the interaction with the retrofitted infill walls [25]. Recent studies have shown the reliability of the available numerical models in predicting the shear demand in frame members caused by the interaction with the infill, both employing macro or micro modelling approaches [26–29]. On the other hand, the complex behaviour of retrofitted infill walls might require more advanced numerical modelling approaches, which allow to account for all the possible failure modes. For instance, the simulation of the interface interaction between masonry substrate and retrofit layer is required to account for cohesive failure, which is a common failure mode in case of FRP retrofit [30].

A numerical model for the simulation of the in-plane response to lateral loads of an infilled RC portal frame is developed in this study. Two infill types are considered, namely an unreinforced masonry wall and a masonry wall retrofitted with fibre-reinforced-polymer layers. The cross section and the reinforcement of

the RC frame members were defined according to a simulated gravity load design, assuming the considered frame as part of the first floor in a four-storey building. This approach allowed to reproduce the configuration of existing buildings, characterized by low performance under seismic actions. Aiming to accurately simulate the failure modes of the analysed frames, a meso-modelling approach is adopted, explicitly defining the brick units in the wall, as well as the interface interaction with the RC frame and the retrofit. The model developed for the masonry wall is firstly validated by simulating diagonal compression tests previously performed at university of Salento [31]. The lateral behaviour of the case study RC portal frames was investigated by mean of non-linear static analyses, to evaluate the failure modes, the energy dissipation and the displacement capacity depending on the infill properties.

2 DESCRIPTION OF THE CASE STUDY PORTAL FRAMES

The portal frame considered in this study replicates the first floor in a 4-storey and 4-bay RC building designed for gravity loads, with bay length, $\boldsymbol{L}$, equal to 5.4 m in both directions and floor height, $\boldsymbol{h}$, equal to 3 m. The dead and live loads on the slab were assumed equal to 5.8 kN/m^2 and to 2.0 kN/m^2, respectively. The cross section of the columns was designed computing the axial load through to the tributary area method, while the beam's cross-section was assumed equal to $\boldsymbol{L}$/10. The longitudinal and transverse reinforcement was defined according to the gravity load design provisions of the Italian building code [32]. The mechanical properties assumed for concrete and reinforcing steel are provided in **Table 1**.

Concrete	
Compressive strength f_c [MPa]	27.0
Young's modulus E_c [MPa]	32306.0
Tensile strength f_{ct} [MPa]	2.7
Reinforcing steel	
Yielding strength f_{ys} [MPa]	450.0
Young's modulus E_s [MPa]	210000.0

Table 1. Mechanical properties of concrete and steel rebars assumed for the numerical model.

In **Table 2**, a description of the analyzed frames is provided. An identification code is assigned to each frame depending on the considered configuration (URF = Frame with UnReinforced infill; FRPF = Frame with Fiber-Reinforced-Polymer infill). The portal frame in its two configurations considered in this study is illustrated in **Figure 1**. The infill wall was composed of tuff stone bricks typical of southern Italy, whose properties were defined based on laboratory tests previously conducted at University of Salento [31]. The compressive strength, $\boldsymbol{f_{cw}}$, and the elastic modulus, $\boldsymbol{E_w}$, were equal to 13.9 MPa and 7796 MPa, respectively. The bed joints were characterized by cementitious mortar with low mechanical properties, to simulate the behaviour of infill walls in existing old buildings.

ID	Column cross section [mm]	Beam cross section [mm]	Infill thickness [mm]	Infill retrofit type
URF	400x400	400x500	200	none
FRPF	400x400	400x500	200	FRP Layer

Table 2. ID of the case study frames.

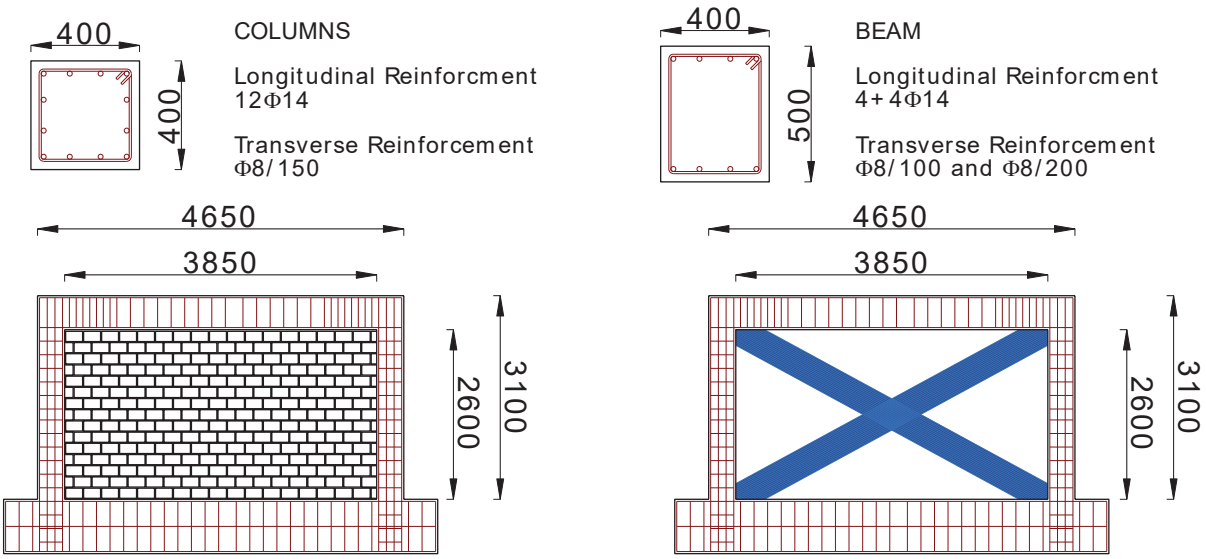

(a) (b)

Figure 1. Configuration of the case study frames: (a) ***URF*** and (b) ***FRPF***.

2.1 Simulated design of the retrofit

The FRP retrofit of the infill wall is composed of diagonal basalt-fibre composite sheets with thickness, t_{FRP}, and width, b_{FRP}, equal to 0.14 mm and 650 mm, respectively. The tensile strength, f_{FRP}, and the elastic modulus, E_{FRP}, were equal to 2326 MPa and 75.98 GPa, respectively. The wall retrofit was designed by replicating a realistic scenario in which a lateral strengthening of the infill is required to avoid severe in-plane cracking in case of earthquake. A target lateral shear strength of the wall, F_{hw}, was computed based on the seismic base shear demand, F_h, defined according to the equivalent static approach described in the Italian building code [32]:

$$F_h = \frac{S_a(T_1) \cdot \lambda \cdot W_b}{q_b} \tag{1}$$

In equation (1), W_b is the total weight of the building, q_b is the behaviour factor, λ is the participating mass coefficient and $S_a(T_1)$ is the spectral acceleration corresponding to the first period of the structure.

The behaviour factor was assumed equal to 1.5 to assume a low ductility of the frame, in consistency with the gravity load design. The value of $S_a(T_1)$ was defined based on a high seismic hazard zone in Italy and considering a design return period equal to 475 years, as prescribed in the Italian building code for residential buildings [32].

The value of F_{hw} was calculated as $F_{hw} = \alpha_w \cdot F_h/[n_w \cdot (\alpha_w+1)]$, being α_w the infill-to-frame relative elastic stiffness (equation (2) and n_w the number of infill walls in the considered direction. This approach assumes that the total base shear in the building is distributed among the RC columns and the infill walls along the perimeter, proportionally to the lateral stiffness of each element.

$$\alpha_w = \frac{n_w G_w t_w l_w h_c^3}{n_c 12 E_c I_c h_w} \tag{2}$$

In equation (2), l_w and h_w are the length and the height of the infill wall, respectively; E_c, I_c and h_c are the elastic modulus of the concrete (computed according to Italian building design code [32]), the moment of inertia of the cross section and the height of the columns, while n_c is the number of columns oriented in the considered direction. It is worth mentioning that the approach adopted for the evaluation of F_{hw} assumes the masonry infill walls as part of the lateral loads resisting system.

Based on the target shear strength, the retrofit was designed adopting simplified formulations provided in the literature. The shear strength of the retrofitted infill, F_{FRP}, was computed according to CNR-DT 200/2013 [14]:

$$F_{hw} \leq F_{FRP} = \tau_w \cdot A_w + F_{f,FRP} \tag{3}$$

In equation (3), τ_w and A_w are the shear strength and the cross sectional area of the infill wall, respectively, $F_{f,FRP}$ is the shear strength contribution provided by the composite, defined through equation (4), depending on the elastic modulus (E_f) the thickness (t_f) and the fracture energy (Γ_f) of the FRP layer.

$$F_{f,FRP} = 0.48 \cdot l_w \cdot 2t_f \cdot \sqrt{\frac{2 \cdot E_f \cdot \Gamma_F}{t_f}} \tag{4}$$

3 NUMERICAL MODEL DESCRIPTION

A three-dimensional model was developed in ABAQUS [33] for the simulation of the lateral behaviour of the infilled portal frames (**Figure 2**). The RC frame members were modelled using eight-node linear elements (C3D8R) with embedded trusses (T3D2), representing concrete and reinforcement rebars, respectively. A simplified elastic-perfectly plastic behaviour in compression was assumed for concrete, where the elastic stress limit was equal to the compressive strength, f_c, and the ultimate strain, ε_{cu}, was computed according to Italian building code [32]. The tensile behaviour featured a linear elastic branch up to the tensile strength, f_{ct}, followed by tension stiffening. Referring to reinforcing steel, an elastic-perfectly plastic behaviour was assumed both in compression and tension, assuming strain at failure, ε_{su}, equal to 0.075.

A discrete meso-modelling approach was adopted for the masonry infill wall, explicitly defining the brick units in the geometry. The mesh of the bricks was characterized by eight-node linear elements

(C3D8R), with linear elastic mechanical behaviour, since their high compressive strength suggested the unlikely occurrence of crushing failure. To validate this statement, the maximum stress in the brick was checked at the end of each simulation performed.

A cohesive law was adopted at the brick-to-brick interface, to simulate the presence of mortar joints (**Figure 2**). The interface behaviour in tension and in the two shear directions was characterized by a linear elastic response up to maximum strength, followed by linear softening, simulating cracking evolution. The damage initiation is ruled by the maximum stress criterion provided in equation (5):

$$max\left\{\frac{t_n}{t_{nL}}, \frac{t_{s1}}{t_{s1L}}, \frac{t_{s2}}{t_{s2L}}\right\} = 1 \tag{5}$$

where t_n, t_{s1} and t_{s2} are the stress values in the three principal directions and t_{nL}, t_{s1L} and t_{s2L} are the limit values when the separation is either purely normal to the interface or purely in the first or the second shear direction, respectively. The tensile limit, t_{nL}, was assumed equal to 0.26 MPa, based on the results of three-point-bending tests on mortar specimens. The values of t_{s1L} and t_{s2L} correspond to the shear strength of mortar joints, τ_w, which was calibrated based on diagonal compression tests performed at university of Salento, as described in the following section. The elastic slope of the cohesive behaviour in pure tension and pure shear are equal to $k_{ss} = G_{mj}/h_{mj}$ and $k_{nn} = E_{mj}/h_{mj}$, respectively, being E_{mj} and G_{mj} the Young's and shear modulus of mortar and h_{mj} the mortar joints thickness.

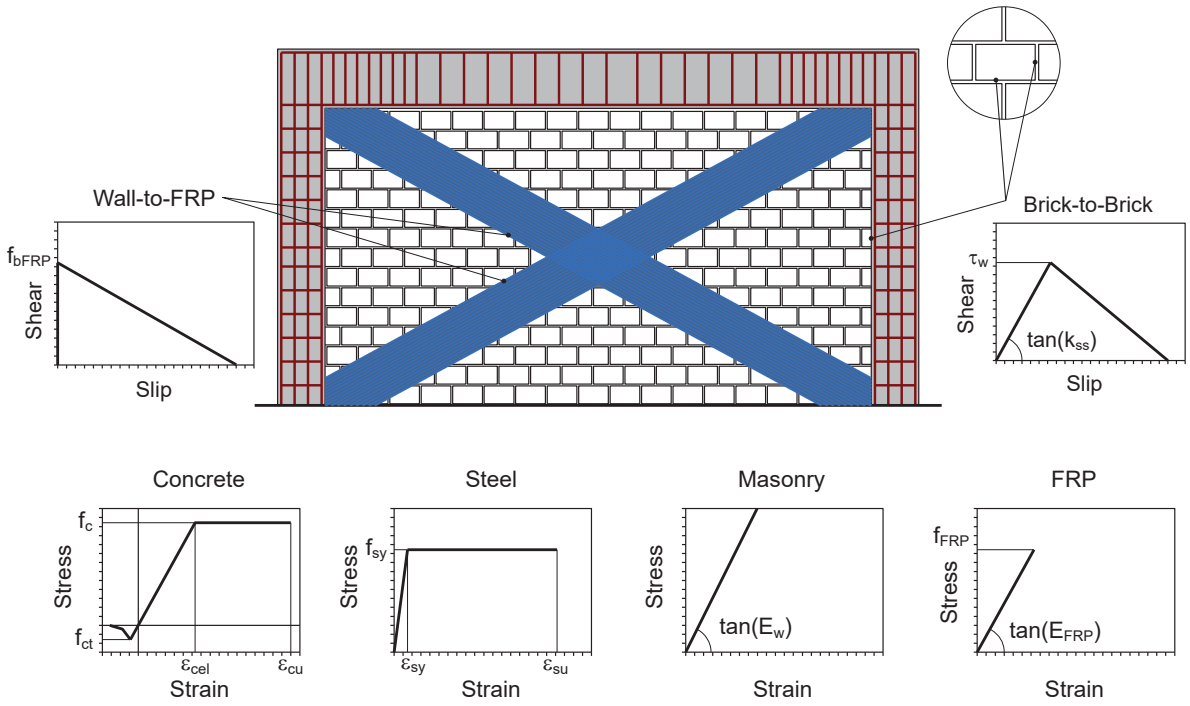

Figure 2. Description of the numerical model.

The damage evolution was defined based on the mixed-mode criterion, representing cohesive failure by equation (6):

$$\frac{G_n}{G_{nL}} + \frac{G_{s1}}{G_{s1L}} + \frac{G_{s2}}{G_{s2L}} = 1 \quad (6)$$

where G_n, G_{s1} and G_{s2} are the energy values in the three principal directions and G_{nL}, G_{s1L} and G_{s2L} are fracture energy values when the separation is either purely normal to the interface or purely in the first or the second shear direction, respectively. As for the shear strength of mortar joints, the fracture energy values were calibrated based on the results of diagonal compression tests described in the following section. In **Figure 2**, the curve representing the cohesive response in pure shear is provided. The same cohesive law was used to simulate the interaction at the wall-frame interface.

The FRP retrofit was modelled through plane surfaces meshed using three-node shell elements (S3). The mechanical stress-strain behaviour of the FRP sheets was composed of a linear elastic branch up to the attainment of the tensile strength, f_{FRP}, followed by tensile failure. Aiming to simulate debonding, a cohesive law was defined at the wall-FRP interface (**Figure 2**). A rigid response was assumed up to failure, followed by linear softening. Since lateral loading mainly produces in-plane internal forces at the interface, no tensile damage was assumed. The shear stress limit, $f_{b,FRP}$, and the fracture energy value were defined based on provisions in CNR-DT 200 R1/2013 [14].

3.1 Calibration of the model adopted for the infill

The model used for the unreinforced and the retrofitted infill was firstly calibrated by simulating diagonal compression tests on masonry specimens. Two tests previously performed at university of Salento on tuff stone masonry walls were selected [31]. The tests setup and the details of the specimens are provided in **Figure 3** and **Table 3**, respectively.

ID	Dimensions [mm]	Masonry type	f_{cw} [MPa]	E_w [MPa]	t_{FRP} [mm]	b_{FRP} [mm]	f_{FRP} [MPa]	E_{FRP} [MPa]
URW	650x650	Tuff stone	13.9	7796.0	-	-	-	-
FRPW	650x650	Tuff stone	13.9	7796.0	0.14	90.0	2326.0	75980.0

Table 3. Specimens' details in diagonal compression tests.

The tests were conducted according to the ASTM E 519-02 standard [34] and were aimed at characterizing the in-plane strength of tuff stone masonry walls typical of Southern Italy. The specimens were composed of 11 layers of masonry bricks with dimensions equal to 100x50x100 mm and cementitious mortar joints of about 10 mm thickness. It is worth noting that the mechanical properties of the masonry wall and the FRP retrofit are the same described in section 2.1.

A monotonic force-controlled loading protocol was applied along the diagonal direction of the specimens through a manually-operated hydraulic jack. The restrained corners of the wall were cut to uniformly distribute the applied load on a plane surface. The diagonal deformations of the specimens were monitored

through linear variable displacement transducers (LVDT), placed at both sides along the two diagonals of the walls. An additional LVDT was also placed at each side to detect possible out-of-plane displacements.

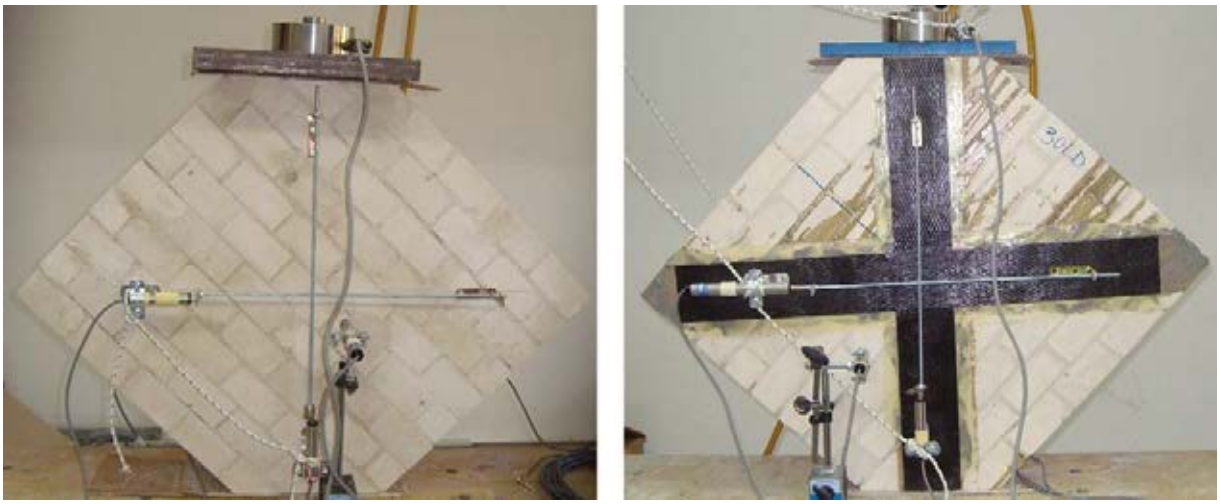

(a) (b)

Figure 3. Test setup for (a) ***URW*** and (b) ***FRPW***.

The response of ***URW*** specimen to diagonal compression was characterized by a brittle failure caused by shear cracking of mortar joints. An off-diagonal cracking path was observed (**Figure 4a**), starting from the corner of the loaded surface. Additionally, geometry imperfections in the specimen caused a minor out-of-plane failure mode. This aspect is evidenced by the significant difference between the displacement measurements provided the vertical LVDTs at the two sides of the wall (LVDT sx and LVDT dx, respectively). The Load-displacement curve is provided in **Figure 5a**. The maximum strength, $\boldsymbol{F_{m,test}}$, and the corresponding displacement, $\boldsymbol{D_{m,test}}$, were equal to 21.5 kN and 0.32 mm, respectively.

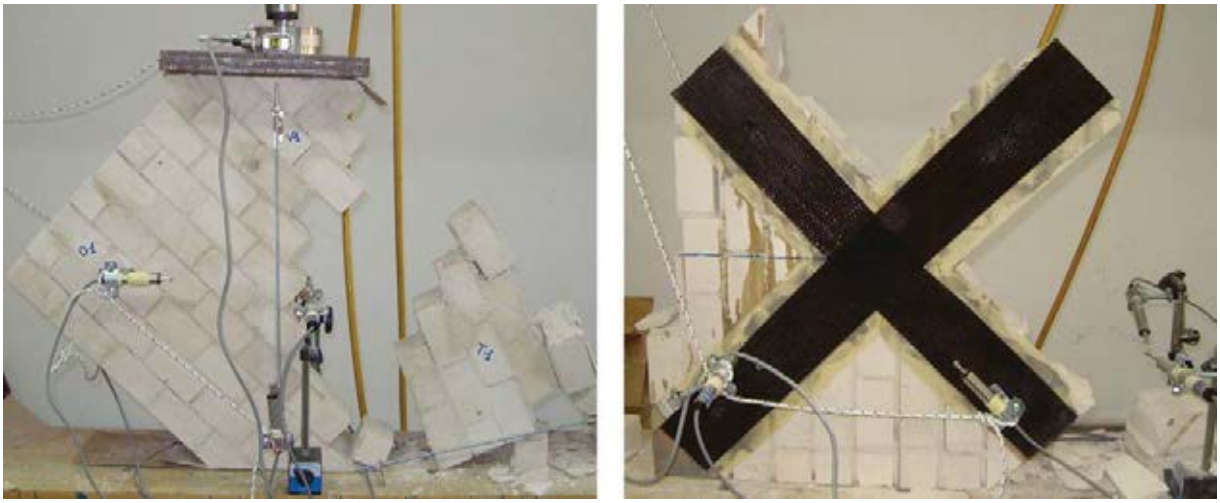

(a) (b)

Figure 4. Failure in case of (a) ***URW*** and (b) ***FRPW***.

In the case of ***FRPW*** specimen, the failure mode was characterized by cohesive debonding of the FRP layer at both sides of the wall, followed by collapse (**Figure 4b**). The presence of retrofit significantly enhanced both the maximum strength and the displacement capacity with respect to the unreinforced

configuration. The values of $F_{m,test}$ and $D_{m,test}$ were equal to 53.1 kN (+146% with respect to ***URW***) and 0.71 mm (+ 296% with respect to ***URW***), respectively. Consequently, a significant increase of the cumulative energy dissipated, ***ED***, was obtained in the case of retrofitted wall, as shown in **Table 4**.

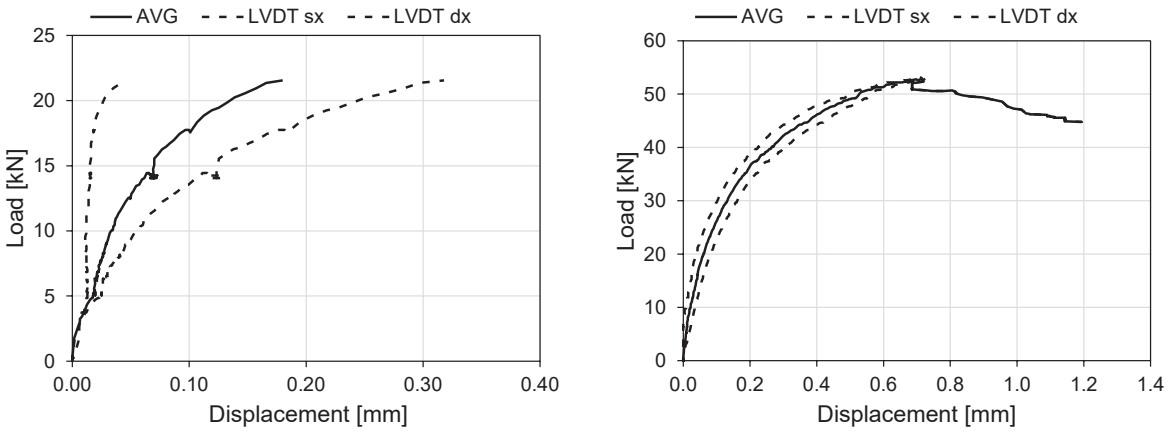

(a) (b)

Figure 5. Load-displacement curves obtained for (a) ***URW*** and (b) ***FRPW***.

In the numerical model, the boundary conditions were simulated by including translational restraints in the three-principal directions and a displacement-controlled vertical load at the bottom and the top surface of the wall, respectively (**Figure 6**). The fracture energy and the shear limit values in the cohesive laws employed for the brick-to-brick and the wall-to-FRP interaction were adjusted to obtain a satisfactory matching of the experimental Load-displacement curves. The comparison between the numerical and the experimental results is provided in **Figure 7**, while the failure modes obtained in the numerical simulations are shown in **Figure 8**. In the case of ***URW***, a satisfactory matching of the linear elastic slope of the experimental curve was obtained, up to a load value equal to 12 kN. Nevertheless, the progressive slope reduction observed in the test, caused by out-of-plane failure, was not simulated by the numerical model. It is worth reminding the unsymmetric vertical displacement measurements provided by the LVDTs placed at opposite sides of the wall, which suggest a significant influence of the specimen's imperfections on the test results. Being this feature not replicated in the numerical model, an accurate match of the post-elastic phase of the curve was not possible.

ID	$F_{m,test}$ [kN]	$D_{m,test}$ [mm]	ED_{test} [kNmm]
URW	21.5	0.18	2.76
FRPW	53.1	0.71	51.93

Table 4. Diagonal compression tests results.

On the other hand, a satisfactory agreement was obtained in terms of maximum strength, displacement capacity and, consequently, cumulative energy dissipated. The difference between the experimental and numerical maximum strength ($F_{m,test}$ and $F_{m,FEM}$, respectively) was equal to 4.8%. The displacement corresponding to the maximum strength in the numerical simulation ($D_{m,FEM}$) was equal to 0.17 mm, that is 5.5% lower compared to $D_{m,test}$. The failure mode in numerical simulation was characterized by minor diagonal cracking followed by bed joint sliding (**Figure 8a**). The difference between numerical and experimental results can be related to the specimen imperfections. Furthermore, it is worth evidencing that

the actual mortar joint thickness was not explicitly included in the numerical model, possibly causing a different path of internal forces comparing to the test.

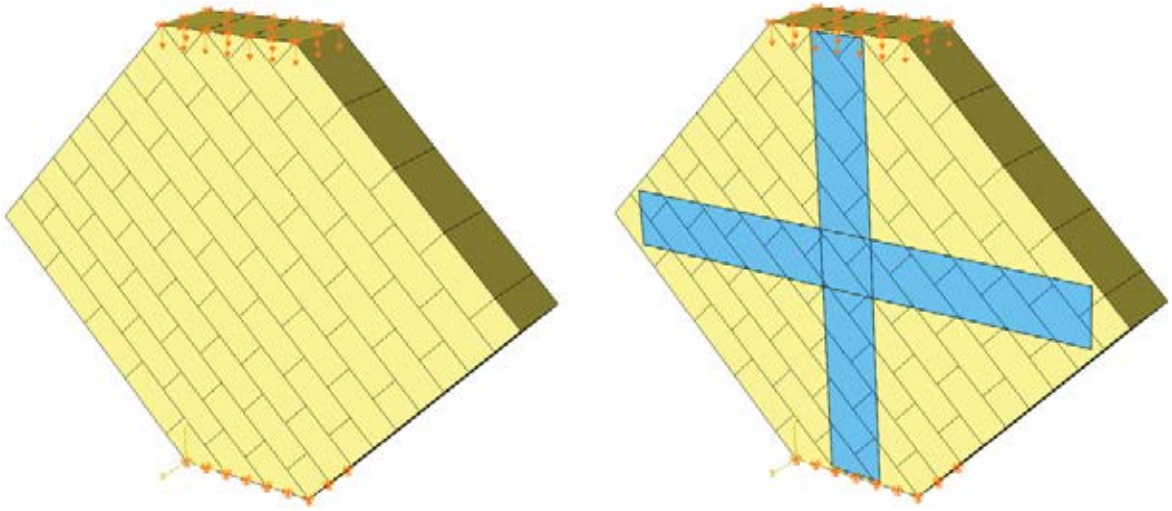

(a) (b)

Figure 6. Numerical model for the simulation of the diagonal compression tests: (a) ***URW*** and (b) ***FRPW***.

In the case of ***FRPW***, both elastic and post-cracking response were precisely simulated by the numerical model, resulting in a satisfactory matching of the energy dissipation capacity up to the maximum strength. The curve obtained from the numerical simulation is characterized by a first, minor debonding of the FRP layer, followed by a redistribution of the internal forces at the wall-FRP interface and stiffness restoration up to failure (**Figure 8b**). Despite the neglectable difference between the numerical and the experimental value of F_m (+1.0%), the numerical model was unable to simulate the post-peak response and the displacement capacity of the specimen. The value of $D_{m,FEM}$ was 23.7% higher than $D_{m,test}$, while the difference between numerical and experimental ***ED*** at failure was equal to 23.65%. This result is probably due to the high complexity of the failure mode of FRP-retrofitted wall, which can be highly influenced by imperfections, such as uneven adhesion of the FRP layer on the wall surface.

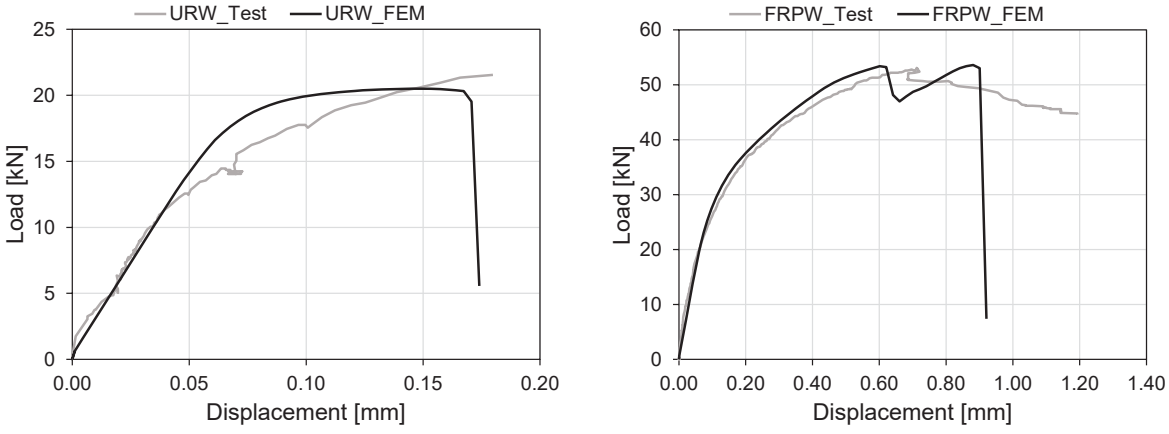

(a) (b)

Figure 7. Comparison between numerical and experimental Load-displacement curves for (a) ***URW*** and (b) ***FRPW***.

The calibrated values of the fracture energy and the shear limit in the cohesive laws employed for the brick-to-brick and the wall-to-FRP interaction were used in the finite element model developed for the simulation of the lateral behaviour of the infilled frames. The same properties as the diagonal compression tests specimens were assumed for masonry brick units and FRP retrofit. The wall thickness was modified from 100 mm to 200 mm, in order to reproduce the configuration of infill walls in full-scaled portals.

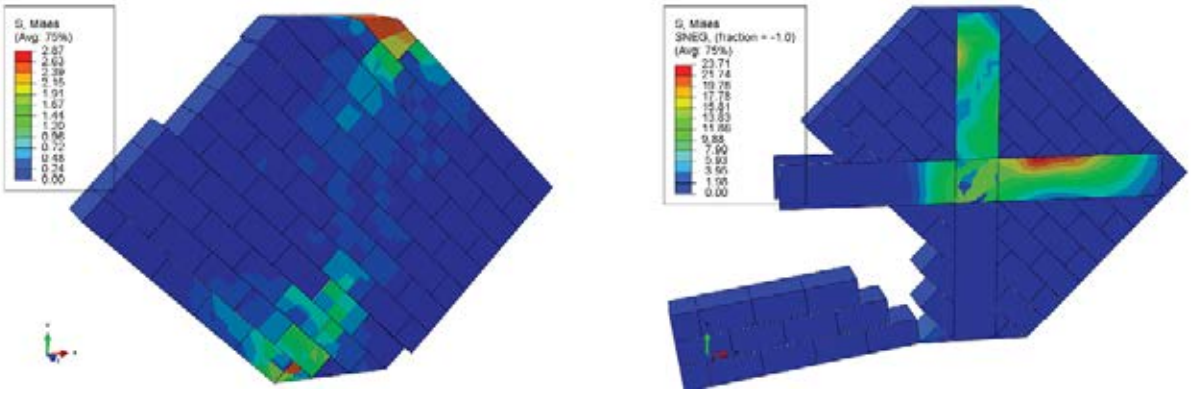

(a) (b)

Figure 8. Failure modes in numerical simulation for (a) ***URW*** and (b) ***FRPW***.

4 PUSHOVER ANALYSIS OF THE FRAMES

The pushover analysis of the frames was performed considering a horizontal displacement-controlled loading protocol, applied to the top of the portal frame. The displacement amplitude was increased up to the achievement of the maximum value Δ_{max}, assumed equal to $\theta_{u,c} \cdot h_c$, being $\theta_{u,c}$ the expected ultimate chord rotation of the columns, computed using equation (7) provided in Eurocode 8 [35].

$$\theta_{u,c} = 0.825 \cdot 0.016 \cdot h_c \cdot (0.3^{\nu}) \left[\frac{max(0.01;\omega')f_c}{max(0.01;\omega)}\right]^{0.225} \left(\frac{L_v}{h_c}\right)^{0.35} 25^{\left(\alpha\rho_{sx}\frac{f_{yw}}{f_c}\right)} \quad (7)$$

In the equation (7), ν is the axial load ratio, ω and ω' are the reinforcement index for tensile and compressive longitudinal rebars, f_c is the cylindrical compressive strength of the concrete, L_v is the shear span, α is the confinement coefficient, ρ_{sx} and f_{yw} are the transverse reinforcement ratio and tensile strength, respectively. The value of Δ_{max} can be reasonably assumed as an upper displacement limit, since the presence of the masonry infill walls generally reduces the displacement capacity of RC frames with respect to a bare configuration.

The lateral load-displacement response and the failure modes of the analysed frames is reported in **Figure 9** and **Figure 10**, respectively. It is worth mentioning that the shear failure of the RC frame members was not detectable by the modelling approach developed, since the mechanical model used for concrete does not account for material degradation under shear. Therefore, the occurrence of the shear failure was assessed by comparing, for each column, the maximum of shear obtained from the analysis to the analytical shear strength, V_{Rc}. The value of V_{Rc} was computed according to the variable inclination strut model [36].

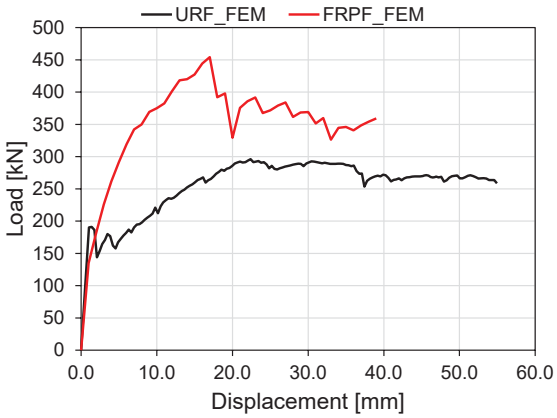

Figure 9. Lateral response of the analysed portal frames.

As shown in **Figure 9**, the maximum lateral strength, F_m, was 53.4% higher in case of ***FRPF*** compared to ***URF***. On the other hand, the contribution of the FRP layer to the elastic stiffness is neglectable. In the case of ***FRPF***, retrofit debonding was observed after the attainment of F_m, at a displacement amplitude equal 17 mm. Referring to ***URF***, the onset of damage in the infill wall was characterized by mortar joints cracking, followed by the generation of a strut mechanism. The maximum strength was attained for a displacement amplitude equal to 22.4 mm, while the post-peak behaviour featured mortar bed joints sliding. The strut mechanism generation, representing the compression field in the wall, leads to an uneven shear distribution among the two columns. This phenomenon is more noticeable in the case of ***FRPF***, since the presence of the retrofit delays the cracking generation in mortar joints, as shown in **Figure 11**.

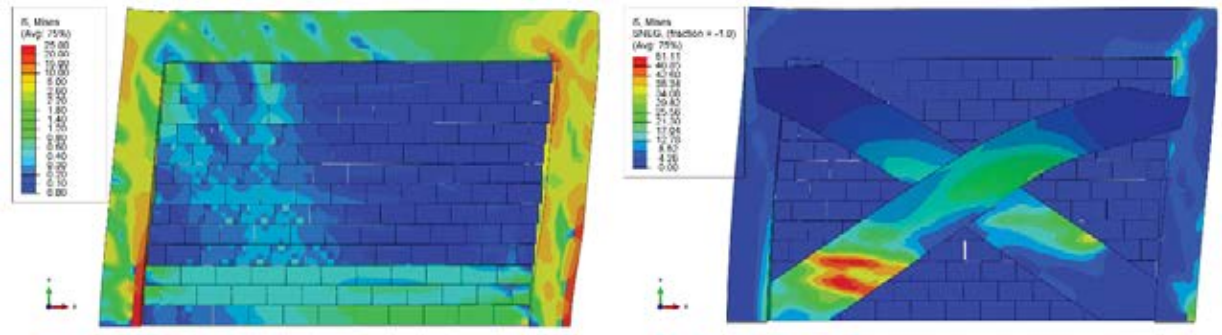

(a) (b)

Figure 10. Failure modes in numerical simulation for (a) ***URF*** and (b) ***FRPF***.

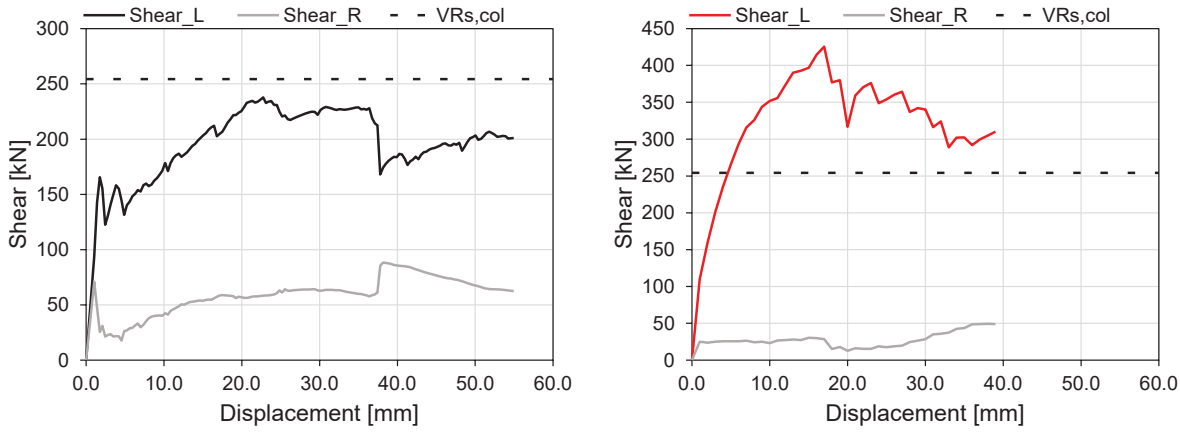

Figure 11. Shear-displacement response obtained for both columns (Shear_L and Shear_R) in case of (a) ***URF*** and (b) ***FRPF***.

The maximum shear in the column in case of retrofitted infill was 67% higher than the shear strength of the column, suggesting early shear failure (**Figure 11b**). Additionally, the displacement amplitude corresponding to the attainment of the shear strength of the column was equal to 4.5 mm, namely 73% lower compared to the debonding displacement. In the case of ***URF***, the value of V_{Rc} was higher than the maximum shear (**Figure 11a**), suggesting a ductile failure mode of the frame and, consequently, higher displacement and energy dissipation capacity compared to ***FRPF***. The comparison of the cumulative energy dissipated up to failure (ED_{SF}), provided in **Figure 12**, evidences the high influence of the retrofit on the performance of the infilled frames analysed. The value of ED_{SF} decreases by 93.2% comparing ***URF*** to ***FRPF*** results.

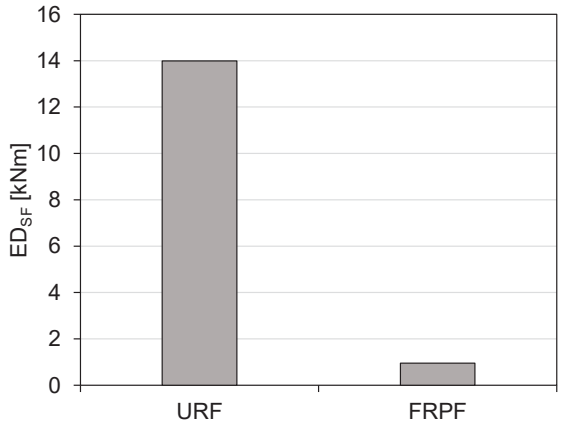

Figure 12. Energy dissipation capacity up to failure of the analysed portal frames.

5 CONCLUSIONS

The influence of infill walls on the seismic performance of RC buildings has been widely demonstrated in the literature. The presence of infill walls characterized by high shear strength can significantly increase the shear demand in the columns, leading to possible premature shear failure in RC frames without adequate structural detailing. The use of FRP to avoid the out-of-plane failure of masonry infills, as well as to improve

their in-plane capacity is commonly adopted nowadays. However, this retrofit intervention is often not designed accounting for the interaction between the infill wall and the surrounding RC frame.

In this study, the response of a masonry infilled RC portal frames designed for gravity load was analysed. Two configurations were considered. The first one was characterized by unreinforced masonry infill, while in the second configuration, FRP retrofit of the of the infill was assumed. A non-linear static analysis was performed on the considered frames, aiming to assess the influence of the infill retrofit on the maximum strength, the displacement and the energy dissipation capacity.

A three-dimensional numerical model was developed, including interface interaction laws between the brick units, at the frame-infill and at the infill-retrofit interface. The interaction laws were calibrated based on diagonal compression tests on tuff stone specimens previously performed at University of Salento. The scope of the modelling approach was the accurate evaluation of the internal forces' distribution, as well as the simulation of the main mechanisms characterizing the lateral response of the analysed infilled frames.

The comparison between numerical and experimental results, referred to the diagonal compression tests, showed a high reliability of the developed finite-element models in simulating the shear response of unreinforced and retrofitted masonry walls. A satisfactory agreement was obtained in terms of maximum shear strength, elastic stiffness and failure modes. The numerical model accurately reproduced the mortar bed joints sliding and the debonding of the FRP retrofit from the wall surface.

The results of the non-linear static analyses carried out on the RC portal frames showed a significant difference in the lateral response of the considered configurations. A ductile failure mode was observed in the case of unreinforced infill, featuring flexural failure of the columns, while the introduction of the FRP reinforcement led to a severe reduction of the ductility capacity of the structure. Despite the increase of the maximum lateral strength caused by the retrofit, early brittle failure of the columns was observed.

The results of this study pointed out the importance of accounting for the interaction between RC frame and infill walls when retrofit techniques, which increase the capacity of the masonry infills, are adopted. Further studies are still required to define design prescriptions which regulate the seismic retrofit of infill walls with composite materials in existing RC buildings.

ACKNOWLEDGEMENTS

This work was supported by "The Laboratories University Network of Seismic Engineering" (RELUIS) under Grant DPC-RELUIS 2019-2021.

REFERENCES

[1] Dhakal RP (2010): Damage to non-structural components and contents in 2010 Darfield earthquake. *Bulletin of the New Zealand Society for Earthquake Engineering*, **43** (4), 404–11.

[2] Perrone D, Calvi PM, Nascimbene R, Fischer EC, Magliulo G (2018): Seismic performance of non-structural elements during the 2016 Central Italy earthquake. *Bulletin of Earthquake Engineering*, 1–23.

[3] Verderame GM, Ricci P, De Luca F, Del Gaudio C, De Risi MT (2014): Damage scenarios for RC buildings during the 2012 Emilia (Italy) earthquake. *Soil Dynamics and Earthquake Engineering*, **66**, 385–400.

[4] Messali F, Ravenshorst G, Esposito R, Rots J (2017): Large-scale testing program for the seismic characterization of Dutch masonry walls. *16th World Conference on Earthquake*, Santiago Chile, p. Paper N° 4753.

[5] Pujol S, Fick D (2010): The test of a full-scale three-story RC structure with masonry infill walls. *Engineering Structures*, **32** (10), 3112–21.

[6] Butenweg C, Marinković M, Salatić R (2019): Experimental results of reinforced concrete frames with masonry infills under combined quasi-static in-plane and out-of-plane seismic loading. *Bulletin of Earthquake Engineering*, **17**, 3397–422.

[7] Celarec D, Ricci P, Dolšek M (2012): The sensitivity of seismic response parameters to the uncertain modelling variables of masonry-infilled reinforced concrete frames. *Engineering Structures*, **35**, 165–77.

[8] Di Trapani F, Bertagnoli G, Ferrotto MF, Gino D (2018): Empirical Equations for the Direct Definition of Stress–Strain Laws for Fiber-Section-Based Macromodeling of Infilled Frames. *Journal of Engineering Mechanics*, **144** (11), 04018101.

[9] Facconi L, Minelli F, Giuriani E (2018): Response of infilled RC frames retrofitted with a cementitious fiber-mesh reinforced coating in moderate seismicity areas. *Construction and Building Materials*, **160**, 574–87.

[10] Koutas L, Bousias SN, Triantafillou TC (2015): Seismic Strengthening of Masonry-Infilled RC Frames with TRM: Experimental Study. *Journal of Composites for Construction*, **19** (2), 04014048.

[11] Altin S, Anil Ö, Kopraman Y, Belgin Ç (2010): Strengthening masonry infill walls with reinforced plaster. *Proceedings of the Institution of Civil Engineers: Structures and Buildings*, **163** (5), 331–42.

[12] Corradi M, Borri A, Castori G, Sisti R (2014): Shear strengthening of wall panels through jacketing with cement mortar reinforced by GFRP grids. *Composites: Part B*, **64**, 33–42.

[13] Erol G, Taskin K, Yuksel E, Karadogan HF (2005): Strengthening of infilled RC frames by CFRP. *WIT Transactions on the Built Environment*, **81**, 591–600.

[14] Consiglio Nazionale delle Ricerche (2013): *Istruzioni per la Progettazione, l'Esecuzione ed il Controllo di Interventi di Consolidamento Statico mediante l'utilizzo di Compositi Fibrorinforzati*. Italy.

[15] Consiglio Superiore dei Lavori Pubblici (2018): *Linea Guida per la identificazione, la qualificazione ed il controllo di accettazione di compositi fibrorinforzati a matrice inorganica (FRCM) da utilizzarsi per il consolidamento strutturale di costruzioni esistenti*. Italy.

[16] Perrone D, Leone M, Aiello MA (2016): Evaluation of the infill influence on the elastic period of existing RC frames. *Engineering Structures*, **123**, 419–33.

[17] Huang H, Burton H V., Sattar S (2020): Development and Utilization of a Database of Infilled Frame Experiments for Numerical Modeling. *Journal of Structural Engineering*, **146** (6), 04020079.

[18] FEMA 356 (2000): *FEMA 356 Prestandard and Commentary for the Seismic Rehabilitation of Building*. Federal Emergency Menagement Agency.

[19] Jeon J-S, Park J-H, DesRoches R (2015): Seismic fragility of lightly reinforced concrete frames with masonry infill. *Earthquake Engineering and Structural Dynamics*, **44**, 1783–803.

[20] Burton H, Deierlein G (2013): Simulation of Seismic Collapse in Non-Ductile Reinforced Concrete Frame Buildings with Masonry Infills. *Journal of Structural Engineering*, **140** (8), A4014016.

[21] Blasi G, Perrone D, Aiello MA (2020): Influence of the modelling approach on the failure modes of RC Infilled frames under seismic actions. *Lecture Notes in Civil Engineering - Proceedings of Italian Concrete Days 2018*, vol. 42, Springer.

[22] Blasi G, Perrone D, Aiello MA (2018): Fragility functions and floor spectra of RC masonry infilled frames: influence of mechanical properties of masonry infills. *Bulletin of Earthquake Engineering*, **16**, 6105–6130.

[23] Madan A, Reinhorn AM, Mander JB, Valles RE (1997): Modeling of Masonry Infill Panels for Structural Analysis. *Journal of Structural Engineering*, **123** (10), 1295–302.

[24] Blasi G, De Luca F, Aiello MA (2018): Brittle failure in RC masonry infilled frames: The role of infill overstrength. *Engineering Structures*, **177**, 506–18.

[25] Blasi G, Perrone D, Aiello MA, Fleischman R (2020): Retrofit of masonry infills: local interaction with RC frames. *Proceedings of the 17th world conference on Earthquake Engineering*, p. Paper N 3e-0019.

[26] Cavaleri L, Di Trapani F (2015): Prediction of the additional shear action on frame members due to infills. *Bulletin of Earthquake Engineering*, **13** (5), 1425–54.

[27] Redmond L, Stavridis A, Kahn L, DesRoches R (2018): Finite-Element Modeling of Hybrid Concrete-Masonry Frames Subjected to In-Plane Loads. *Journal of Structural Engineering*, **144** (1), 04017178.

[28] Akhoundi F, Lourenço PB, Vasconcelos G (2014): Numerical Modelling of Masonry-Infilled Reinforced Concrete Frames: Model Calibration and Parametric Study. *9th International Masonry Conference (9IMC2014)*.

[29] Pantò B, Caliò I, Lourenço PB (2017): Seismic safety evaluation of reinforced concrete masonry infilled frames using macro modelling approach. *Bulletin of Earthquake Engineering*, **15** (9), 3871–95.

[30] Marcari G, Manfredi G, Prota A, Pecce M (2007): In-plane shear performance of masonry panels strengthened with FRP. *Composites Part B: Engineering*, **38** (7–8), 887–901.

[31] Leone M, Sciolti MS, Aiello MA (2012): In-plane shear behavior of BFRP reinforced masonry panels. *Proceeding of the New boundaries in the application of FRP composites in Civil Engineering - 6th International Conference on FRP composites in civil engineering*, Rome (IT).

[32] NTC-2018 (2018): *Aggiornamento delle «Norme tecniche per le costruzioni»*. D.M. 17 Gennaio 2018, Italy.

[33] Dassault Systemes (2016): *Abaqus Theory Manual*.

[34] ASTM E 519-02 (2002): *Standard Test Method for Diagonal Tension (Shear) in Masonry Assemblages*. American National Standard.

[35] EN 1998-3 (2005): *Eurocode 8 - Design of structures for earthquake resistance - Part 3: Assessment and retrofitting of buildings*. European Standard.

[36] Fardis MN (2009): *Seismic design, assessment and retrofitting of concrete buildings*. Springer.